Water Research 223 (2022) 118984

Contents lists available at ScienceDirect

Water Research

journal homepage: www.elsevier.com/locate/watres

Oxidation of organic micropollutant surrogate functional groups with peracetic acid activated by aqueous Co(II), Cu(II), or Ag(I) and geopolymer-supported Co(II)

Tero Luukkonen [a,b,*], Urs von Gunten [b,c,*]

[a] University of Oulu, Fibre and Particle Engineering Research Unit, P.O. Box 8000, FI-90014, Finland
[b] Eawag, Swiss Federal Institute of Aquatic Science and Technology, Überlandstrasse 133, Dübendorf CH-8600, Switzerland
[c] School of Architecture, Civil and Environmental Engineering (ENAC), Ecole Polytechnique Lausanne (EPFL), Lausanne 1015, Switzerland

ARTICLE INFO

Keywords:
Advanced oxidation process
Oxidant-reactive functional groups
Peracetic acid
Transition metal catalysts
Water treatment
Geopolymer

ABSTRACT

Peracetic acid (PAA) in combination with transition metals has recently gained increasing attention for organic micropollutant abatement. In this study, aqueous Co(II), Cu(II), and Ag(I) were compared for their capacity to activate PAA. Co(II) outperformed Cu(II) or Ag(I) and the optimum conditions were 0.05 mM of Co(II), 0.4 mM of PAA, and pH 3. However, due to a wider applicability in water treatment, pH 7 (i.e., bicarbonate buffer) was selected for detailed investigations. The abatement of different micropollutant surrogates could be described with a second-order rate equation (observed second-order rate constants, k_{obs} were in the range of 42–132 M^{-1} s^{-1}). For the *para*-substituted phenols, there was a correlation between the observed second-order rate constants of the corresponding phenolates and the Hammett constants (R^2 = 0.949). In all oxidation experiments, the reaction rate decreased significantly after 1–2 min, which coincided with the depletion of PAA but also with the deactivation of the Co(II) catalyst by oxidation to Co(III) and subsequent precipitation. It was demonstrated that Co(II) immobilized on a geopolymer-foam performed approximately similarly as aqueous Co(II) but without deactivation due to Co(III) precipitation. This provides a potential option for the further development of heterogeneous catalytic Co(II)/PAA advanced oxidation processes utilizing geopolymers as a catalyst support material.

1. Introduction

Oxidation processes have been successfully implemented in water and wastewater treatment for disinfection and oxidation purposes in the last > 100 years (von Gunten, 2018). A large selection of chemical oxidants such as chlorine, ozone, chlorine dioxide, permanganate and advanced oxidation processes are routinely applied but all of them have shortcomings in terms of feasibility, efficiency and the formation of potentially problematic oxidation/disinfection byproducts (DBPs, such as aldehydes, epoxides, halogenated compounds, or *N*-nitrosamines) (von Gunten, 2018). Peracetic acid ($CH_3C(O)OOH$, PAA) might be a promising alternative because of its low tendency to form DBPs under typical water treatment conditions (Henao et al., 2018). PAA is available as an equilibrium solution with hydrogen peroxide and acetic acid and it is used as an oxidizing, disinfecting, and sterilizing agent in several industries. In wastewater treatment, PAA has gained a niche market as a disinfectant and its application is projected to grow (Bettenhausen, 2020). The disinfection efficiency of PAA is comparable to sodium hypochlorite for some common bacterial indicators (e.g., *Escherichia coli, Pseudomonas* sp., *Salmonella* sp., and *Clostridium perfringens*) and protozoa (e.g., *Giardia* cysts) while a lower efficiency was reported for a viral indicator (e.g., coliphage viruses) (Briancesco et al., 2005; Veschetti et al., 2003). The disinfection mechanism of PAA is based on its oxidative damage of bacterial cell membranes (Wang et al., 2020), enzymes (Lazarova et al., 1998), and DNA (Buschini et al., 2004; Zhang et al., 2019). H_2O_2 plays a synergistic role in the PAA-based disinfection once PAA has damaged microorganisms partially and inactivated the catalase enzyme (Flores et al., 2014).

In addition to disinfection, there is a growing interest to utilize PAA for the oxidation of refractory aqueous micropollutants (Ao et al., 2021). However, it is known that PAA reacts very selectively with electron-rich organic moieties (Chen et al., 2022; Dong et al., 2021; Kim and Huang,

* Corresponding authors at: Eawag, Swiss Federal Institute of Aquatic Science and Technology, Überlandstrasse 133, Dübendorf CH-8600, Switzerland.
E-mail addresses: tero.luukkonen@oulu.fi (T. Luukkonen), urs.vongunten@eawag.ch (U. von Gunten).

https://doi.org/10.1016/j.watres.2022.118984
Received 20 May 2022; Received in revised form 25 July 2022; Accepted 13 August 2022
Available online 14 August 2022

2021). The oxidation occurs via an oxygen atom transfer of PAA to electron-rich sites of the target compounds (Kim and Huang, 2021). The second-order rate constants for the reactions between PAA and organic compounds vary over more than 10 orders of magnitude (10^{-6}–10^{5} M^{-1} s^{-1}) and they decrease in the following order: S-containing compounds > phenols > N-containing compounds > alkenes > aldehydes (Kim and Huang, 2021). In comparison to ozone, a widely applied chemical oxidant, the corresponding second-order rate constants are significantly lower (von Sonntag and von Gunten, 2012), and thus it has been demonstrated that when PAA is used directly (i.e., without activation), it is relatively ineffective for degrading a large range of diverse micropollutants (Hey et al., 2012).

In the last decades, advanced oxidation processes (AOPs) have been implemented to overcome the shortcomings of conventional chemical oxidants, and thus AOPs such as O_3/H_2O_2, UV/H_2O_2 and UV/Cl_2 have been used to tackle a larger range of micropollutants (Stefan, 2018). Similarly, the reactivity of PAA towards organic micropollutants can be enhanced by using it in different AOPs, that is, by combining it with, for example, ultraviolet (UV) irradiation, ultrasound, activated carbon, or transition metal catalysts to enhance the formation of radicals (Ao et al., 2021). One appealing feature of PAA is the relatively low O-O bond energy of 38 kcal mol^{-1}, while it is 51 kcal mol^{-1} for H_2O_2, and thus PAA is easier to activate (Bach et al., 1996; Bianchini et al., 2002). Additionally, PAA has a lower unoccupied molecular orbital (LUMO) energy (i.e., it can more readily accept electrons) in comparison to H_2O_2, -0.25 eV vs. 0.57 eV, respectively (Kim et al., 2019).

The oxidation mechanism of PAA depends on the selection of the activation method. For instance, the primary radicals from UV/PAA are hydroxyl ($^{\bullet}OH$) and acetyloxyl ($CH_3C(O)O^{\bullet}$) radicals that form upon the homolytic O-O bond cleavage (Caretti and Lubello, 2003; Lubello et al., 2002). These primary radicals react further with PAA, acetic acid, or H_2O_2 and the radicals with the highest steady-state concentrations when using typical commercial PAA compositions are $^{\bullet}OOCH_2C(O)O^{-}$, $^{\bullet}OOCH_3$, and $CH_3C(O)OO^{\bullet}$ (Zhang and Huang, 2020). Of several transition metals, Co(II) has received a great deal of interest recently to activate PAA: it reacts with PAA ($k = 1.70 \times 10^{1}$–6.67×10^{2} M^{-1} s^{-1} in the pH range 3.0–8.2) resulting in the formation of $CH_3C(O)O^{\bullet}$ and $CH_3C(O)OO^{\bullet}$ (Kim et al., 2020; Wang et al., 2020). Of these, acetylperoxyl (i.e., $CH_3C(O)OO^{\bullet}$) is the main radical contributing to micropollutant oxidation (Kim et al., 2020; Wang et al., 2020). For the reaction of Fe(II) with PAA ($k = 1.10 \times 10^{5}$–1.56×10^{4} M^{-1} s^{-1} in the pH range 3.0–8.1), the main radicals are $CH_3C(O)O^{\bullet}$, $^{\bullet}OH$, and additionally oxo-iron complexes (e.g., $Fe^{IV}O^{2+}$) are formed (Kim et al., 2019). The reduction of Fe(III) by PAA is slow ($k = 2.72$ M^{-1} s^{-1}), and thus the use of 2,2′-azino-bis(3-ethylbenzothiazoline-6-sulfonate) (ABTS) has been proposed to aid in the reduction of Fe(III) via the formation of reactive $ABTS^{\bullet+}$ (in that case, $k = 1.3 \times 10^{2}$ M^{-1} s^{-1}) (Lin et al., 2021). However, using Fe(II)/Fe(III) is limited to low pH (≤ 3.5) since Fe(III) hydrolyzes and forms precipitates at higher pH (Stumm and Morgan, 1996).

The above-mentioned metals have been studied in various immobilized forms (i.e., as heterogeneous catalysts), including Fe(II)-containing zeolite (Wang et al., 2020), Co_3O_4 (Wu et al., 2020), and $CoFe_2O_4$ (Dong et al., 2022; Wang et al., 2021). In this context, novel catalyst supports for PAA activation could be geopolymer foams, which resemble conventional ceramics but are synthesized at mild conditions (20–100°C temperature and ambient pressure) without sintering. Several industrial alkaline, silicate or aluminosilicate side-streams can be used as their raw materials and the material properties (e.g., specific surface area, porosity, and ion-exchange capacity) are promising for catalyst applications (Novais et al., 2020). So far, they have been used in several studies as a support media in photocatalysis but rarely in other types of oxidative treatments for water or wastewater (Zhang et al., 2020).

The objectives of this study were to (i) compare aqueous Ag(I), Cu(II), and Co(II) for their capability to activate PAA for the oxidation of micropollutant surrogate compounds under realistic conditions with stable pH in buffer solutions, (ii) optimize the conditions for oxidation (i.e, catalyst concentration, pH, and PAA concentration) by using phenol as a target compound, (iii) perform kinetic experiments using the optimized conditions for differently substituted phenols, aniline, primary, secondary and tertiary amines, and an olefin covering typical oxidizable organic moieties in micropollutants and evaluate whether quantitative structure–activity relationships could be established, (iv) obtain information about the stability of the Co(II) catalyst under the studied conditions (e.g., by a multiple PAA dosage experiment), and (v) assess the suitability of a foamed geopolymer as a novel metal-catalyst support for PAA-based oxidative water treatment. Ag(I) and Cu(II) were selected for this study as they have been investigated sparsely in earlier studies related to PAA-based AOPs, while Co(II)/PAA is rather well characterized, and thus it served as a reference AOP system.

2. Materials and methods

2.1. Chemical reagents

Industrial-grade PAA (tradename Proxitane 12:20, Solvay, Finland; composition: 12% PAA, 20% H_2O_2, 20% acetic acid, and 0.5–1% H_2SO_4 as w/w) was used in all experiments. The model compounds (Table S1, Supporting Information (SI)) were selected as surrogates for micropollutants based on the presence of electron-rich moieties, which can be oxidized by chemical oxidants (Lee and von Gunten, 2010). Phenolic compounds were selected to investigate the effect of electron-withdrawing (fluoro, chloro, cyano, and nitro) and electron-donating (methyl) groups in *para* position and additionally a trisubstituted phenol (2,4,6-trichlorophenol) was investigated. Primary, secondary and tertiary amines (i.e., benzylamine, *N*-methylbenzylamine, or *N,N*-dimethylbenzylamine, respectively) and aniline were selected as representatives of reactive nitrogen-containing moieties. Cinnamic acid was selected as an olefinic compound, which can also be attacked by electrophiles. Other reagents employed in this study are described in Text S1 (SI). All stock solutions and dilutions were prepared in ultrapure water (Milli-Q Ultrapure Water System, Millipore).

2.2. Analysis of peracetic acid and hydrogen peroxide concentrations

PAA and H_2O_2 were quantified with a two-stage spectrophotometric method (modified from Domínguez-Henao et al. (2018) and Bader et al. (1988)) for which the details are provided in Text S2 (SI). In short, the analyte solution was combined with phosphate buffer, potassium iodide, and *N,N*-diethyl-p-phenylenediamine (DPD) solutions. PAA oxidized iodide to iodine (Awad et al., 2003; Shah et al., 2015), which then oxidized DPD. The oxidation product of DPD was quantified by measuring the absorbance at 551 nm, which quantifies the PAA concentration. In the second stage, a peroxidase solution was added to catalyze iodide oxidation by H_2O_2 (Bader et al., 1988). Again, the absorbance was measured at 551 nm, which quantifies the total concentration of peroxides. The H_2O_2 was then determined by subtraction of the PAA concentration from the total peroxide concentration. The first and second absorbances were always read after 30 and 60 s, respectively, after adding the reagents.

2.3. Analysis of micropollutant concentrations

Micropollutant concentrations were measured by liquid chromatography equipped with mass spectrometer (LC-MS) using an Acquity UPLC system (Waters) connected to a Q Exactive Plus mass spectrometer (ThermoFisher). 5 μL samples were injected into an Atlantis Premier BEH C18 AX 1.7 μm 2.1 × 100 mm column (Waters) and eluted with a gradient consisting of 10 mM ammonium acetate at pH 9 and acetonitrile. The flow rate was 0.5 μL min^{-1} with 5% of acetonitrile for 2 min; at 2.1 min, acetonitrile was increased to 40% and kept for 2 min; then raised to 90% in 0.5 min; and returned to the initial conditions at 5 min.

Mass spectra were recorded in negative polarity using the parallel reaction monitoring mode with normalized collision energy of 10 V to isolate ions at m/z 93 with a 2 Da window, resolution of 17500, maximum injection time of 500 ms and automatic gain control set at 1×10^6.

Raw data were processed with the Xcalibur Software (Thermo Fisher) and its Quan Browser option to quantify ions at 93.0330 (10 ppm window). Quadratic calibration curves for each surrogate micropollutant were established with standards including calibration blanks (Text S2, SI).

2.4. Preparation of geopolymer foam containing Co(II)

The geopolymer foam was prepared according to Luukkonen et al. (2020), where the physical, chemical, and morphological characterization of the foam is reported in detail. In short, alkali-activator solution containing 87 weight-% of a sodium silicate solution (Merck, Germany, $SiO_2 \approx 27$ weight-%, $Na_2O \approx 8$ weight-%) and 13 weight-% of NaOH pellets (VWR Chemicals, Sweden) was prepared 24 h before use. Then, metakaolin (MetaMax, BASF, Germany) and the alkali activator were mixed in a weight ratio of 1.00 : 1.36 for 5 min using an overhead stirrer (speed 2000 rpm). H_2O_2 (VWR Chemicals, France, 30% w/w) and Triton X-100 surfactant (Sigma-Aldrich, France) were added as 1.75 and 0.12 weight-% of the mixture, respectively, and mixing (2000 rpm) was continued for 2 min. The mixture was poured into a plastic column (with a height of 99mm and a diameter of 44mm), allowed to consolidate at 60°C for 4 h, and kept in a plastic bag at room temperate after that. On the following day, a capillary impregnation method was applied to introduce Co(II): the pore volume of the foam was filled with a 0.1 M cobalt acetate pentahydrate solution and allowed to stand for 24 h. During this time, Na^+ in the geopolymer was exchanged with Co(II) (Niu et al., 2022). The foam was flushed with 1 L of ultrapure water by pumping it through the foam with a peristaltic pump (flowrate 1 L h^{-1}). The foam was stored at room temperature in a plastic bag before use.

2.5. Oxidation of micropollutants

The oxidation experiments were conducted in brown 25 mL glass flasks containing 15 mL of solution except for kinetic experiments, which were performed in a beaker protected from light containing 1000 mL of solution. Surrogate micropollutants, catalysts, and PAA solutions were added to the flasks or beakers, and they were mixed with a reciprocating shaker or magnetic stirrer, respectively, until the targeted reaction time was reached. To stop the experiment, 9% (w/w) aqueous solution of sodium thiosulfate pentahydrate (Merck, Germany) was added to quench PAA (the molar ratio of thiosulfate to PAA was ~4) and Dowex Marathon MSC hydrogen-form cation exchange resin (cation exchange capacity 1.6 meq/mL by wetted bed volume, Sigma Aldrich, USA) was added to remove the metals. The amount of added resin was approximately 1.6 g $mmol^{-1}$ of metals.

The oxidation experiments were initiated by determining the effects of the aqueous catalyst (Cu(II), Co(II), or Ag(I)) concentration in the range of 0.005–1 mM and pH in the range of 3–7. The pH conditions were controlled by using ultrapure water acidified with HNO_3 (65% w/w, Merck, EMSURE®, Germany) (pH = 3), 10 mM malic acid buffer (pH = 5), or bicarbonate buffer (pH = 7). The complexation of the metal catalyst by the buffers was estimated by speciation calculation (Text S3, SI). The surrogate micropollutant employed at this stage was phenol with an initial concentration of 10 μM. The PAA concentration was 0.4 mM with a reaction time of 3 h.

In a second series of oxidation experiments, the PAA concentration was varied in the range of 0.2–1 mM while the other parameters were kept constant: catalyst (either Cu(II) or Co(II)) concentration at 0.05 mM, pH at 7, phenol concentration at 10 μM, and reaction time at 3 h.

Once the optimized pH, catalyst, and PAA concentrations were determined, oxidation kinetics were determined for the selected surrogate micropollutants (phenol, 4-methylphenol, 4-nitrophenol, 4-fluorophenol, 4-cyanophenol, 4-chlorophenol, 2,4,6-trichlorophenol, *N,N*-dimethylbenzylamine, *N*-methylbenzylamine, benzylamine, aniline, and cinnamic acid) with reaction times between 15 s and 6 h. Also, it was studied how two individual doses of PAA (0.4 mM each) affect the surrogate micropollutant abatement if a second dose is added after 1 or 10 min.

PAA and H_2O_2 decay were measured in selected experiments according to the spectrophotometric method described above. In addition, pH and dissolved oxygen concentrations were monitored using a Hach HQ4100 meter equipped with IntelliCal PHC10101 and LDO101 probes, respectively.

The experiments involving the Co(II)-modified geopolymer foam and a reference foam without Co(II) were conducted by pumping bicarbonate buffer solution (pH = 7) containing the surrogate micropollutant (10 μM) and PAA (0.4 mM) through the foam with a peristaltic pump (flowrate 1 L h^{-1}) and taking samples at 15 min intervals up to 1 h and at 1 h intervals up to 7 h. The empty bed contact time in the system was ~9 min. The leaching of Co(II) was monitored by analyzing the samples from the column effluent with inductively coupled plasma mass spectrometry (XSeries II, Thermo Fisher Scientific) following a standard method (SFS-EN ISO 17294-2, 2016). The concentrations of PAA and H_2O_2 were observed as described above.

3. Results and discussion

3.1. Optimization of oxidation conditions

A first set of experiments (Fig. 1) was conducted to find the optimum catalyst among Ag(I), Co(II), or Cu(II), catalyst concentration (range from 0.005 to 1 mM), and pH (3, 5, or 7). Also, the fraction of non-complexed metal was calculated (Text S3, SI).

The use of Ag(I)/PAA has been shown to yield a synergy for disinfection (De Velásquez et al., 2008; Luna-Pabello et al., 2009) but no previous publications are available about micropollutant oxidation. As shown in Fig. 1A, the optimum pH and Ag(I) dose were 7 and 0.01 mM, respectively, but only a maximum of ~20% abatement of phenol was achieved. Although the mechanism is not resolved in detail, it has been proposed that the synergy of Ag(I)/PAA in disinfection could be due to a PAA-induced enhancement of the exposure of bacteria for Ag(I) (Lalueza et al., 2012; Luna-Pabello et al., 2009). The action of PAA alone (in Fig. 1, the symbols with 0 mM of added catalysts) resulted in only ~1% abatement of phenol. Consequently, the observed abatement of phenol could be due to an Ag(I)/H_2O_2 reaction. In a previous study, ~40% abatement of 2,4-dichlorophenol (C_0 = 0.5 mM) was reported with a H_2O_2 concentration of 4 mM (in the present study it was 1.49 mM), an Ag(I) concentration of 1 mM at pH 7 with a contact time of 90 min (Zhou, 2017).

The combination of Cu(II)/PAA can result a synergy for disinfection (Luna-Pabello et al., 2009) and potentially also be used for the oxidation of micropollutants as indicated by a few earlier publications (Luukkonen et al., 2015; Wang et al., 2021). For Cu(II), the optimum phenol abatement was at pH 7 with a catalyst concentration of 0.05 mM (Fig. 1B). In a recent study, a Cu(II)/PAA system (0.015 mM of Cu(II) and 0.06 mM of PAA) was used for triclosan oxidation and the presence of HCO_3^-/CO_3^{2-} (optimum at 5 mM, pH of 9.3) enhanced the abatement rate due to the formed Cu(II)-carbonato complexes (Wang et al., 2021). Based on these findings, the observed higher abatement of phenol at pH 7 (i.e., in the buffer containing 3 mM of HCO_3^-) in comparison to pH 3 or 5 could also be explained by the formation of Cu(II)-carbonato complexes (57% of Cu(II) is complexed under these conditions (Text S3, SI)). At pH 5 and 7, $Cu(OH)^+$ is present as a hydrolysis product. It has been shown by Wang et al. (2021) that Cu(II)/PAA, in absence of HCO_3^-/CO_3^{2-} is a poor oxidant at pH 8.3. At this pH, the concentration of $Cu(OH)^+$ is higher than in the present study (pH = 3–7). Consequently, it appears that $Cu(OH)^+$ does not enhance the oxidation by the Cu(II)/PAA system.

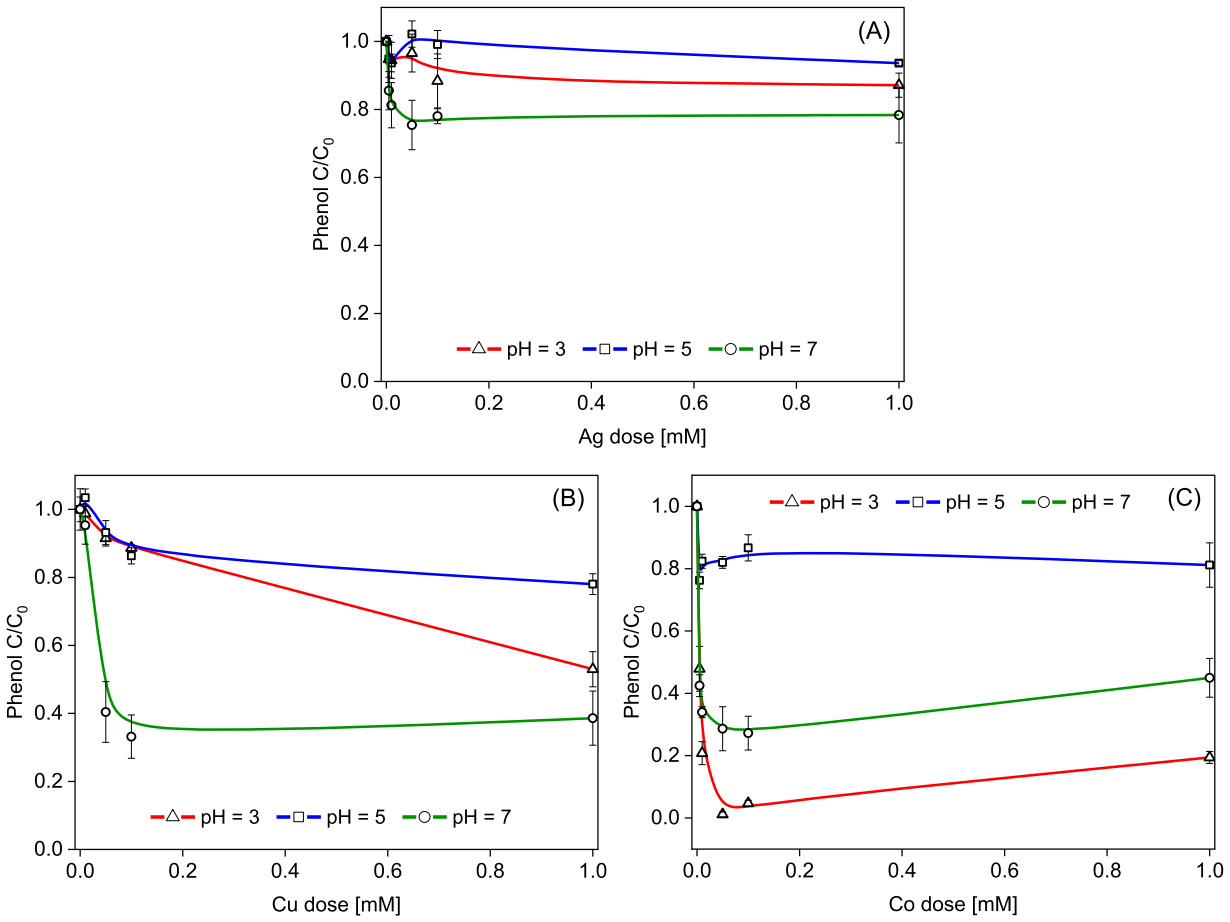

Fig. 1. Effect of pH and catalysts doses ((A) $AgNO_3$, (B) $Cu(NO_3)_2{\cdot}3H_2O$, and (C) $Co(CH_3COO)_2{\cdot}4H_2O$) on the abatement of phenol ($C_0 = 10$ μM) in presence of PAA ($[PAA]_0 = 0.4$ mM). Reaction time was 3 h.

At pH 3, where the concentration of $Cu(OH)^+$ is very low and in absence of malate or CO_3^{2-}/HCO_3^- (i.e., Cu(II) is present mainly as a free Cu^{2+} ion), the abatement efficiency increased as the Cu(II) dose increased. Thus, Cu^{2+} appears to be a more effective catalyst than $Cu(OH)^+$.

In the case of Co(II), ~99% abatement of phenol was observed at pH 3 and a Co(II) concentration of 0.05 mM. The lower performance at pH 5 and 7 is likely due to the Co(II) complexation by malate or CO_3^-/HCO_3^- as only about 26 and 65% of Co(II) is non-complexed, respectively, under the applied experimental conditions. Additionally, Co(II) forms $Co(OH)^+$ in the pH range of the experiments (Schweitzer and Pesterfield, 2010). Furthermore, the higher abatement observed at pH 3 is likely related to a different reaction mechanism in comparison to higher pH (see Section 3.4). Liu et al. (2021) reported that the active oxidizer in the Co(II)/PAA system at low pH is likely Co(IV). The higher abatement rate at pH 7 in comparison to pH 5 could also be due to the presence of peracetate anion ($CH_3C(O)OO^-$, ~6% of total PAA concentration at pH 7, pK_a of PAA is 8.2) with a faster reaction with Co(II) (Coyle et al., 2014). In contrast to Cu(II), the formation of complexes with HCO_3^-/CO_3^{2-} (and malate) appears to be unfavorable for the catalytic activity of Co(II). This was also documented by Wang et al. (2020) who showed that sulfamethoxazole abatement decreased from 90% to 70% and further 60% as HCO_3^- concentration was increased from 0 to 0.2 mM and 0.5 mM, respectively (in the present study, the HCO_3^- concentration was 0.3 mM). Kim et al. (2020) reported that the optimum pH for the AOP involving Co(II)/PAA was 5.0–7.1 but their system was not buffered, and thus the pH decreased ≤ 2.2 units upon the addition of PAA. However, since pH 3 is not techno-economically feasible for most municipal water treatment scenarios, pH 7 was chosen in the subsequent experiments. At that pH, a Co(II) dose of 0.05 mM was the optimum while higher doses up to 1 mM resulted in a less efficient abatement of phenol. Similar behavior has been reported for the Co(II)/PAA process earlier and it is likely due to the scavenging of the radicals at high concentrations of Co(II) (Kim et al., 2020).

Co(II) and Cu(II) concentrations of 0.05 mM at pH 7 were selected for the optimization of the PAA dose using phenol as the target compound (Fig. 2). Co(II) resulted in consistently higher relative abatement of phenol although the difference to Cu(II) decreased with increasing PAA doses. PAA doses > ~0.6 mM resulted in no further improvement in the abatement. This finding is in line with a study of Wang et al. (2020), who reported that PAA doses > 0.4 mM did not lead to improved abatement of sulfamethoxazole, likely due to the scavenging of radicals at high PAA concentrations. Based on this finding, a PAA dose of 0.4 mM was selected for the kinetic experiments.

Solutions containing Co(II) or Cu(II) were also compared by measuring PAA and H_2O_2 decomposition and the evolution of dissolved oxygen as a function of time during oxidation of phenol (Fig. 3). For Co (II), the PAA concentration decreased from 0.39 to 0.04 mM within 1 min and then remained almost constant up to 3 h. The H_2O_2

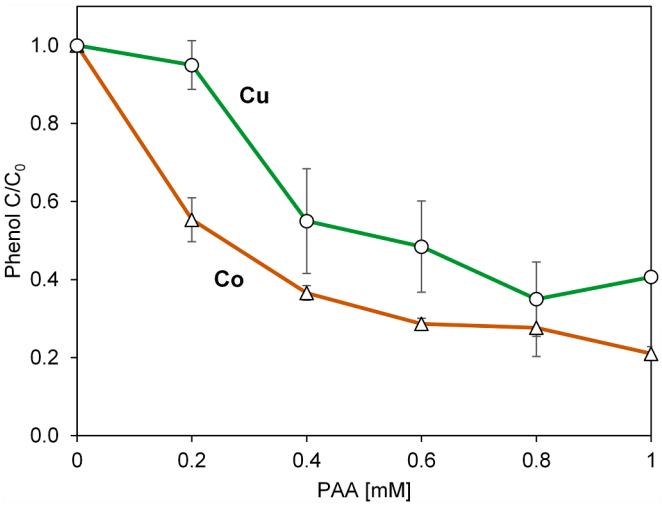

Fig. 2. Effect of PAA concentration on the relative abatement of phenol with Co (II) or Cu(II) catalysts (C_0 (phenol) = 10 μM, $[Co(II)]_0$ and $[Cu(II)]_0$ = 0.05 mM, t = 3 h, pH = 7 ($[HCO_3^-]$ = 3 mM)).

concentration decreased only by ~12% (from 1.24 to 1.09 mM) during the 3 h experiment. The dissolved oxygen concentration increased within ~2 min to a maximum value, followed by a decrease probably due to exchange with the atmosphere (the experiment was conducted in an open vessel). The observed increase in dissolved oxygen concentration (~0.3 mM O_2) is roughly in agreement with the theoretical maximum dissolved oxygen release from PAA and H_2O_2 upon their degradation (i.e., 1/2 mol of O_2 per mol of PAA or H_2O_2). Dissolved oxygen evolution was likely related to a partial loss of PAA via self-decomposition catalyzed by Co(II). Since the concentration of PAA was 40 × compared to the concentration of micropollutant surrogate compounds (i.e., 0.4 mM and 10 μM, respectively), even only a small fraction of PAA reacting to radicals would be sufficient for the observed abatement of the target compounds.

For Cu(II), only ~25% of PAA and no H_2O_2 decomposed over 3 h and, during the first 1 h, no increase in dissolved oxygen was observed. The decomposition of H_2O_2 by Cu(II) is affected by the molar ratio of H_2O_2 and Cu(II), their concentrations, and presence of complexing agents for Cu(II) as shown by Pecci et al. (1997). They demonstrated that when the conditions were similar as in Fig. 3D (pH = 7, [Cu(II)] = 0.05 mM, and $[H_2O_2]$ = 1.2 mM), the oxygen evolution was very low, which is in agreement with our study. According to their results, the H_2O_2 concentration in the present study should have been in higher excess to result in a significant oxygen evolution. Overall, these observations confirm that Co(II) is a much more potent catalyst than Cu(II) in activating PAA.

3.2. Oxidation kinetics

The kinetics of abatement of differently substituted phenols (Fig. 4A-G), an olefin (Fig. 4H), and aniline, primary, secondary, and tertiary amines (Fig. 4I-L) for the optimized oxidation conditions all followed a similar pattern: An initial fast decrease of concentration (duration of

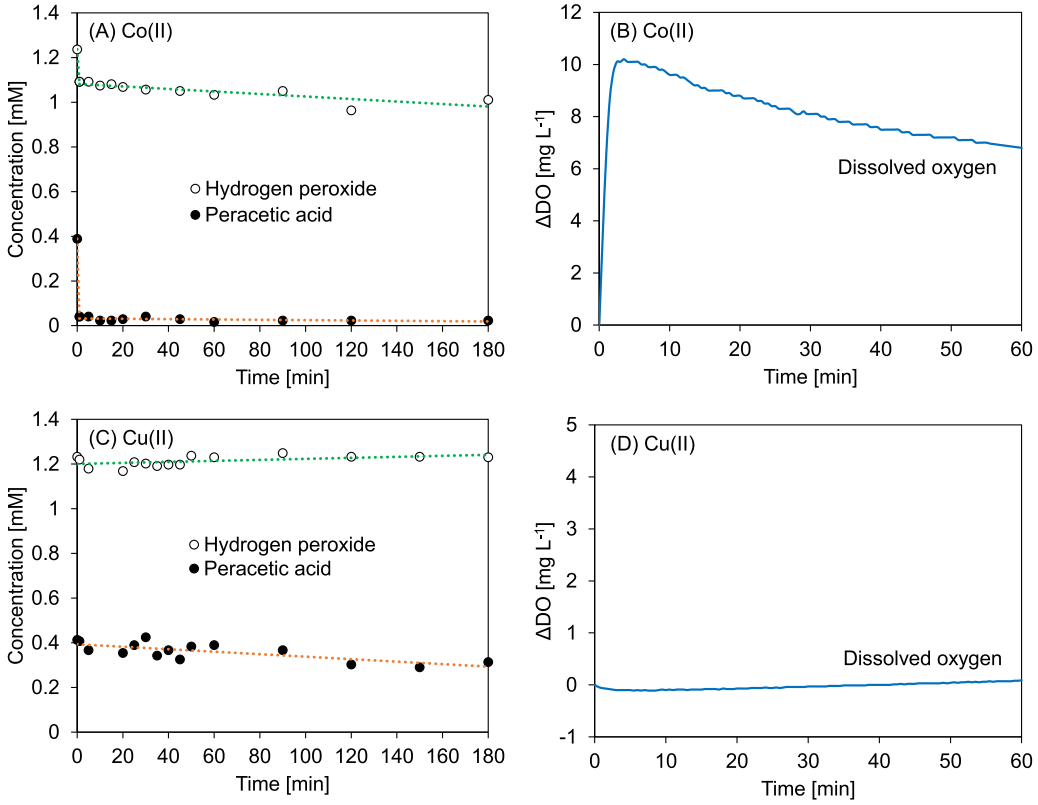

Fig. 3. Evolution of PAA, H_2O_2, and O_2 in Me(II)/PAA systems during oxidation of phenol: (A) Concentrations of PAA and H_2O_2 and (B) change in dissolved oxygen concentration (ΔDO) as a function of time in the presence of Co(II). (C) Concentration of PAA and H_2O_2 and (D) ΔDO as a function of time in the presence of Cu(II). Experimental conditions: C_0 (phenol) = 10 μM, $[Co(II)]_0$ or $[Cu(II)]_0$ = 0.05 mM, $[PAA]_0$ = 0.4 mM, pH = 7 ($[HCO_3^-]$ = 3 mM).

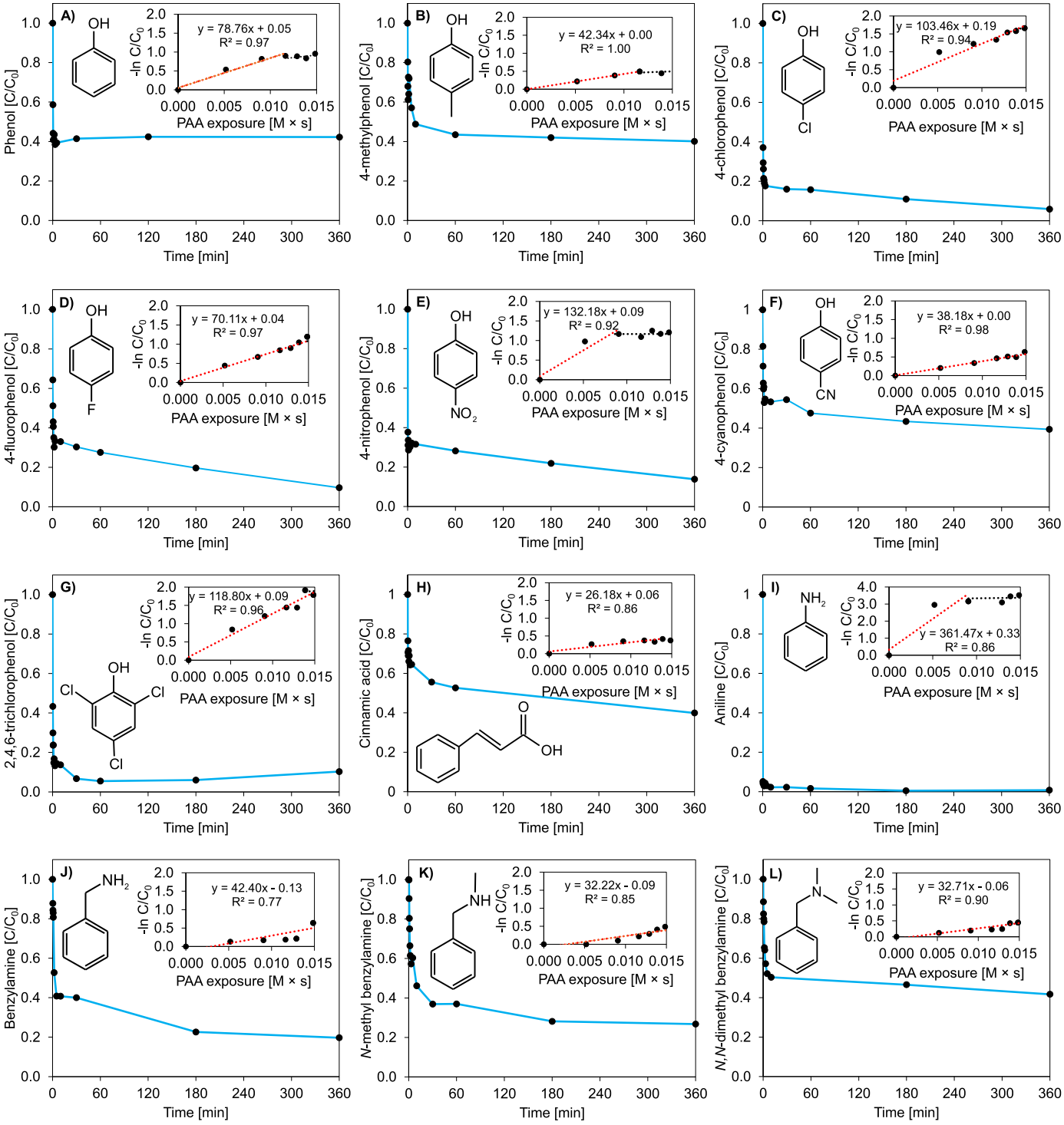

Fig. 4. Degradation of surrogate compounds with various functional groups (A-G: phenols; H: olefin; I: aniline; J-L: primary, secondary and tertiary amines) as a function of time under optimized conditions ($[Co(II)]_0$ = 0.05 mM, [PAA] = 0.4 mM, pH = 7 ($[HCO_3^-]$ = 3 mM)). The insets show the fitting of the data to the a second-order rate equation (Eq. (1)) ($-\ln(C/C_0)$ vs. PAA exposure in M s): the measured reaction rates decrease significantly after 1–2 min (corresponding to PAA exposures of approx. 0.010–0.015 M s).

Table 1
Co(II)/PAA system: Estimated apparent second-order rate constants from an initial reaction time of 1–2 min and % abatement for micropollutant surrogate compounds at pH = 7, $[C]_{0,\ surrogate}$ = 10 μM, $[PAA]_0$ = 0.4 mM, and $[Co(II)]_0$ = 0.05 mM. The second-order rate constants represent only rough estimates, and thus they are rounded to whole numbers.

Surrogate micropollutant	pK_a	Phenolate [%]	Abatement at 60 min [%]	k_{obs} [M^{-1} s^{-1}]	$k_{phenolate}$ [M^{-1} s^{-1}]	$\Sigma\sigma^-_{o,\ m,\ p}$
Phenols						
4-methylphenol	10.3	0.05	60	42	8×10^4	-0.17
Phenol	10.0	0.10	58	79	8×10^4	0
4-fluorophenol	9.9	0.13	72	70	5×10^4	0.06
4-chlorophenol	9.4	0.39	95	103	3×10^4	0.19
4-cyanophenol	8.0	3.28	52	38	1×10^3	0.66
4-nitrophenol	7.2	38.69	70	132	3×10^2	1.27
2,4,6-trichlorophenol	6.2	86.32	84	119	1×10^2	0.57
Amines						
N,N-dimethylbenzylamine	-	-	62	33	-	-
N-methylbenzylamine	-	-	63	32	-	-
Benzylamine	-	-	49	42	-	-
Aniline	-	-	98	361	-	-
Olefin						
Cinnamic acid	4.4	-	47	26	-	-

Phenolate [%] = $100 \times 10^{-pKa}/(10^{-pKa} + 10^{-pH})$; $k_{phenolate} = k_{obs}$ / Phenolate [%]; pK_a values from Hoigné and Bader (1994) and Haynes (2017).

approximately 1–2 min), followed by a slower decrease. The initial fast decrease of the concentrations of the micropollutant surrogate compounds coincided with the observed depletion of PAA (Fig. 3A). The kinetics of micropollutant abatement could be described with a second-order rate equation taking the PAA concentration decrease into account (Eq. 1, in which c is the concentration of micropollutant surrogate compound at time t (s), c_0 is the initial concentration of micropollutant surrogate compound, k_{obs} is the second-order rate constant (M^{-1} s^{-1}), and $\int_0^t [PAA]dt$ is the PAA exposure (M s), i.e., the integral of the curve shown in Fig. 3A. Plots of Eq. 1 are shown in insets of Fig. 4.

$$-\ln\left(\frac{c}{c_0}\right) = k_{obs}\int_0^t [PAA]dt \quad (1)$$

It should be noted that the second-order rate constants reported here are estimates just for comparative purposes (due to the limited data for the PAA evolution), and thus do not reflect absolute second-order rate constants. The observed second-order rate constants for the initial 1–2 min reaction time are provided in Table 1.

For phenolic compounds, the second-order rate constants for the oxidation of phenolates can be expected to be much higher than for neutral phenols (Hoigné and Bader, 1994, 1983; Lee and von Gunten, 2012). Consequently, the rate constants for the oxidation of phenols were considered insignificant for the overall rate expression at near-neutral pH conditions (Jans et al., 2021). The second-order rate constants for the phenolates were plotted against the Hammett coefficients, reflecting electron-withdrawing or donating substituents (Fig. 5) (Hansch et al., 1991). A good correlation could be established for the *para*-substituted phenols (R^2 = 0.949, Fig. 5) but the 2,4,6-trichlorophenol deviated from the trend, indicating likely a different mechanism, because all ortho- and para-positions are substituted.

Cinnamic acid, representing an olefinic surrogate micropollutants, yielded by far the lowest second-order rate constant (Fig. 4H, Table 1). The second-order rate constant of benzylamine (primary amine) was slightly higher than for *N*-methylbenzylamine or *N,N*-dimethyl benzylamine (secondary and tertiary amines), which were approximately similar. In contrast, aniline was abated very effectively and with the highest second-order rate constant of the evaluated compounds. This is due to the activation of the benzene ring and is in line with the easy oxidizability of aniline by other oxidants (Lee and von Gunten, 2010).

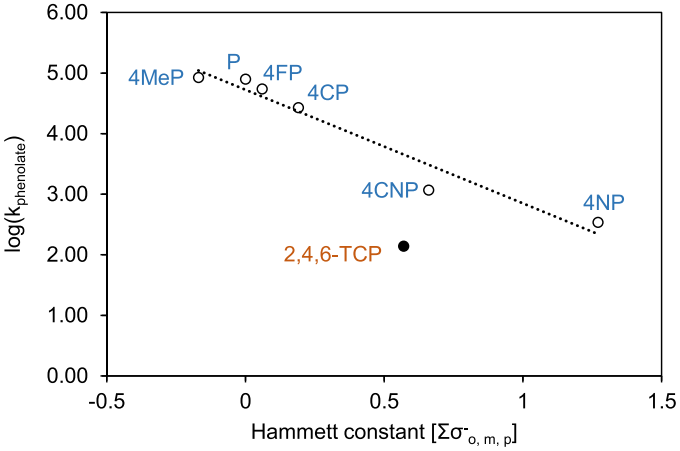

Fig. 5. Correlation between the observed second-order rate constants for the abatement of phenolates (Table 1) and the sum of the Hammett constants ($\Sigma\sigma_{o,\ m,\ p}^-$): y = -1.875x + 4.726, R^2 = 0.949. The kinetics of the abatement of *para*-substitutued phenols (4-methylphenol (4MeP), phenol (P), 4-fluorophenol (4FP), 4-chlorophenol (4CP), 4-cyanophenol (4CNP), and 4-nitrophenol (4NP)) and 2,4,6-trichlorophenol (2,4,6-TCP) were determined in the Co(II)/PAA system for the optimized conditions ($[PAA]_0$ = 0.4 mM, $[Co(II)]_0$ = 0.05 mM, $[phenols]_0$ = 10 μM, pH = 7 ($[HCO_3^-]$ = 3 mM)). Note: 2,4,6-TCP is excluded from the linear regression fitting.

3.3. Test on deactivation of the catalyst

Based on the experimental findings so far, the reaction rates decreased after approximately 1–2 min reaction time, depending on the target compound. This timeframe coincides with the observed depletion of PAA (Fig. 3A), and thus an experiment involving a second addition of PAA (0.4 mM) was conducted with phenol as the target compound (Fig. 6). The second dose of PAA was added after 1 or 10 min reaction

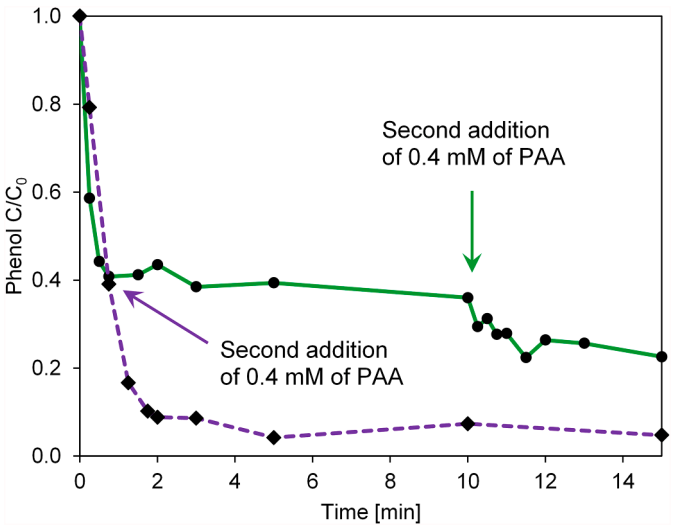

Fig. 6. Abatement of phenol as a function of time with a second addition of PAA at 1 min (dashed purple curve) or 10 min (solid green curve). Experimental conditions: $[PAA]_0 = 0.4$ mM, $[Co(II)]_0 = 0.05$ mM, $[phenol]_0 = 10$ μM, pH = 7 ($[HCO_3^-] = 3$ mM).

time, which resulted in a major or minor additional abatement of phenol compared to the initial reaction, respectively (Fig. 6).

When the reaction in the Co(II)/PAA system was continued for several hours, a finely dispersed precipitate formed. The precipitate was analyzed with X-ray photoelectron spectroscopy (XPS), which indicated the formation of CoO(OH) (Text S4, SI). Thus, it appears that in the studied Co(II)/PAA system, an irreversible formation of Co(III) precipitates takes place. A similar process could also occur in real waters since the bicarbonate concentration is typically approximately similar as in the present system. It should be noted that the Co(III) species precipitating after several hours were likely present as colloids already after 10 min but it took more time for them to coagulate and form visible precipitates. A rapid formation of Co(III) colloids/precipitates is probably the main reason why a second addition of PAA only yields an additional abatement of phenol after 1 min reaction time (Fig. 6). For longer reaction times, Co(III) is completely deactivated in polynuclear complexes.

3.4. Mechanistic considerations

The reaction mechanism occurring in the Co(II)/PAA system has been scrutinized in several previous studies (Kim et al., 2020; Liu et al., 2021; Wang et al., 2020). Therefore, no mechanistic study was performed here, instead we apply information from previous studies to rationalize the results. The dominant radicals contributing for micropollutant abatement have been assessed by radical scavenger experiments and supported by electron spin resonance measurements (Kim et al., 2020; Liu et al., 2021; Wang et al., 2020). The addition of tert-butanol (a commonly used scavenger for $^{\bullet}OH$ (Gao et al., 2021)) to the Co(II)/PAA system did not significantly affect the target compound abatement, and thus it was concluded that $^{\bullet}OH$ plays a minor role (Kim et al., 2020; Liu et al., 2021; Wang et al., 2020). 2,4-hexadiene was used to scavenge $^{\cdot}OH$ ($k \approx 1 \times 10^{10}$ M^{-1} s^{-1}), $CH_3C(O)O^{\bullet}$, and $CH_3C(O)OO^{\bullet}$ (for which second-order rate constants were not available but were assumed to be sufficiently high) from the Co(II)/PAA system and its addition inhibited the abatement of the target compounds very effectively (Kim et al., 2020). However, the role of $CH_3C(O)O^{\bullet}$ was deemed

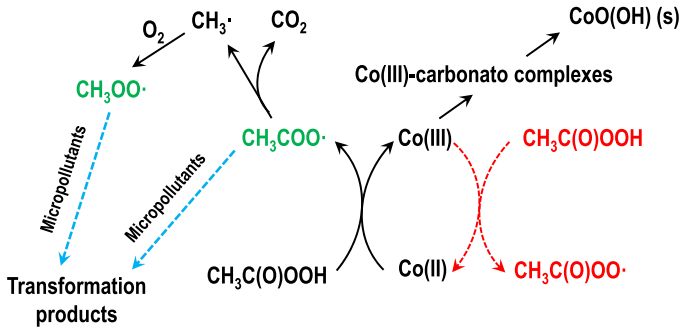

Fig. 7. Schematic representation of the potential main reactions occurring in the Co(II)/PAA system: Under the experimental conditions in this study, the cycling of Co(II)/Co(III) is inhibited due to the precipitation of CoO(OH), thus preventing the formation $CH_3C(O)OO^{\bullet}$ (dashed red lines). The main radicals contributing to the micropollutant abatement are hypothesized to be $CH_3COO^{\bullet}$ and $CH_3OO^{\bullet}$ (highlighted in green) (Kim et al., 2020; Wang et al., 2020).

minor due to a decay into $CH_3^{\bullet}$ and CO_2 ($k = 2.3 \times 10^5$ s^{-1}), and therefore the main species contributing for target compound abatement would be $CH_3C(O)OO^{\bullet}$ (Kim et al., 2020). Other possible radicals such as the superoxide radical, $HO_2^{\bullet}/O_2^{\bullet-}$ ($pK_a = 4.8$), can form from the unimolecular decay of $CH_3C(O)OO^{\bullet}$ ($k = 1.82$ s^{-1}) (Kamath et al., 2018) or from the reaction of H_2O_2 with $CH_3C(O)OO^{\bullet}$, but due to its lower reactivity with organic compounds, it was concluded to play a minor role (Kim et al., 2020). In fact, superoxide is often a reductant for electron-poor compounds (Guo et al., 2021). The decay of $CH_3COO^{\bullet}$ forms $^{\bullet}CH_3$, which can react with O_2 to form $CH_3OO^{\bullet}$ ($k = 4.1 \times 10^9$ M^{-1} s^{-1}) (Kim et al., 2020; Marchaj et al., 1991). However, the oxidation capability of $CH_3OO^{\bullet}$ has been shown to be relatively modest (Neta et al., 1990; Wang et al., 2020).

An efficient cycling between of Co(II) and Co(III) where PAA acts both as electron acceptor and donor (for which the second-order rate constants are 0.17–6.67 $\times 10^2$ M^{-1} s^{-1} and 0.04–4.57 $\times 10^2$ M^{-1} s^{-1}, respectively, at pH 3–5.9) has been hypothesized to be crucial for the Co(II)/PAA process (Kim et al., 2020; Wang et al., 2020). However, based on the evidence shown above (especially in Fig. 6), it appears that the Co(II)-Co(III) cycling is interrupted in the present study due to the formation of insoluble Co(III) precipitates, which causes a limited formation of $CH_3C(O)OO^{\bullet}$, the species deemed the main radical contributing for micropollutant abatement in previous studies. Thus, the mechanism of target compound abatement in the present study could occur via the actions of $CH_3COO^{\bullet}$ and $CH_3OO^{\bullet}$. A scheme of the potential reactions is presented in Fig. 7.

H_2O_2 played a minor role in the studied system since the oxidation of Co(II) to Co(III) ($Eh_0 = -1.84$ V) is thermodynamically favorable by PAA ($Eh_0 = 1.96$ V) but not by H_2O_2 ($Eh_0 = 1.78$ V) (Eberhardt et al., 1993; Luukkonen and Pehkonen, 2017). The observed decrease of H_2O_2 concentration (Fig. 3A) was likely due to H_2O_2 reactions with radicals (Kim et al., 2020) and by a catalytic effect of the formed Co(III) species. A minor role of H_2O_2 in the Co(II)/PAA system was also confirmed by Wang et al. (2020).

3.5. Immobilized catalyst on geopolymer foam

Since the addition of aqueous Co(II) to water treatment systems is not easily possible, immobilized Co(II) could be used to activate PAA. In the present study, a novel support material, a geopolymer foam, was applied. By utilizing such a heterogeneous Co(II)-catalyst, a release of Co(II) to the water phase/environment can be avoided with a convenient

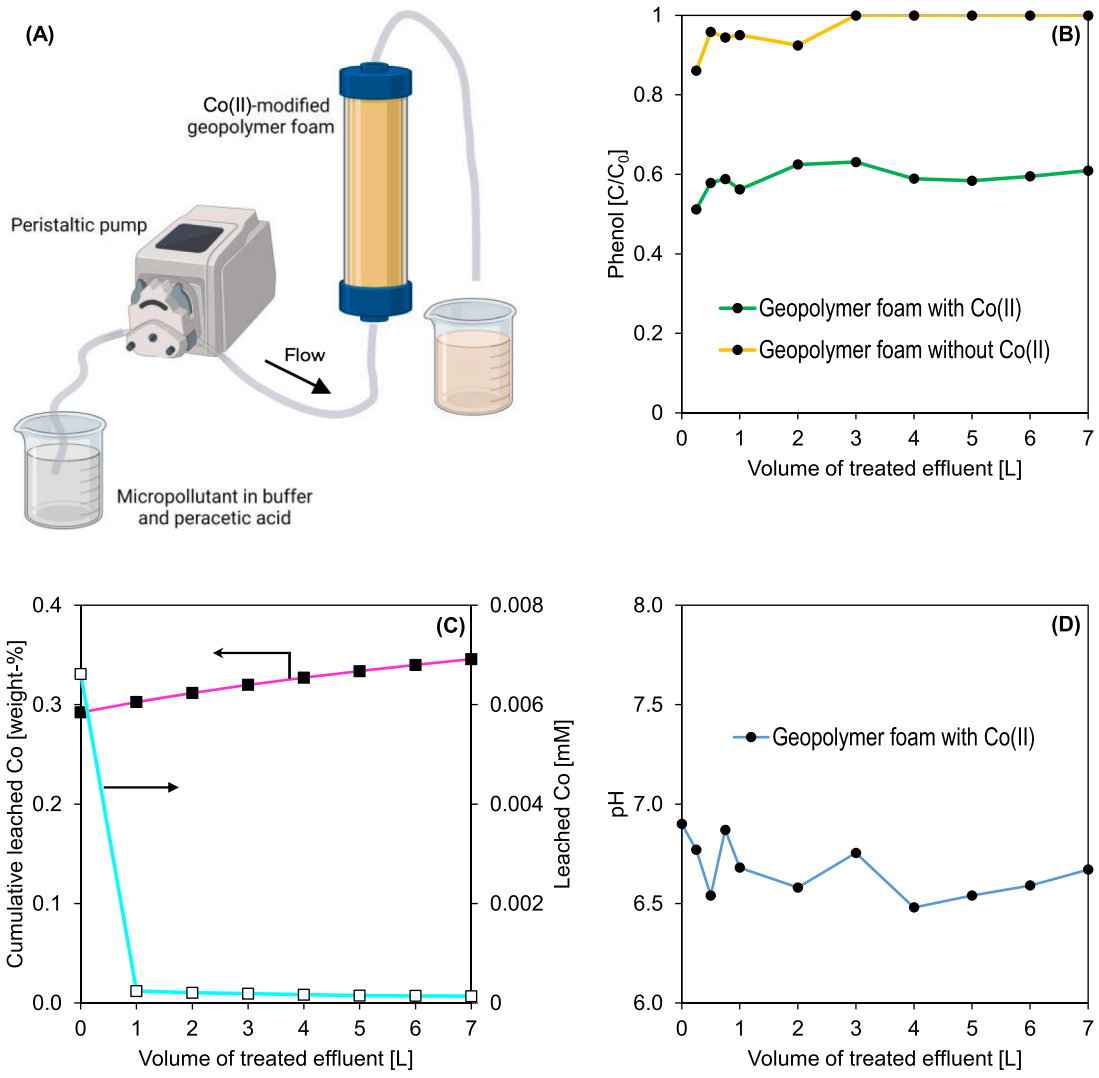

Fig. 8. Heterogeneous Co(II)/PAA experiments. (A) Setup of the experiments involving a Co(II)-loaded geopolymer foam. (B) Relative residual phenol concentrations after geopolymer foam filtration with and without Co(II). (C) Leaching of Co(II) from the Co(II)-modified filter as a function of the filtered volume. (D) Evolution of pH during the experiment. Experimental conditions: Flowrate 1.0 L/h, empty bed volume 0.15 L, empty bed contact time ~9 min, $[PAA]_0 = 0.4$ mM, C_0 (phenol) = 10 μM, and pH = 7 (bicarbonate buffer, $[HCO_3^-] = 3$ mM). Loading of geopolymer was ~2 mg Co/g geopolymer.

recovery and recycling of the catalyst after use. When Co(II) is immobilized on a support material, it could be also less prone for complexation, and thus exhibits higher catalytic activity. Furthermore, a heterogeneous catalyst could help to mitigate problems related to the catalyst deactivation as described above.

Fig. 8A shows the setup used for the continuous heterogenous Co(II)/PAA experiments. The relative abatement of phenol in this system (Fig. 8B) was initially ~50% and then stabilized to a level of ~40%. The geopolymer foam without Co(II) did not abate phenol, confirming that the abatement was due to the interaction of the immobilized Co(II) and PAA. PAA and H_2O_2 concentrations were also depleted during the interaction with Co(II)-containing foam comparable to the homogeneous system (i.e., the PAA concentration decreased consistently from the initial 0.4 mM to 0.04 mM after the column). The leaching of Co(II) decreased sharply after 1 h (Fig. 8C) to a level of < 0.2 μM – a clearly lower concentration than the observed optimum of aqueous Co(II) (0.05 mM). Since the phenol abatement was approximately constant after 1 h, these results imply that there was no catalyst deactivation during the experiments. The Co(II)-containing foam stayed active for the treatment of ~7 L of model solution, which corresponds ~47 empty bed volumes. The pH remained within 6.5–6.9 (the initial pH was 6.9 (Fig. 8D).

4. Conclusions

Co(II) proved to be the most efficient metal ion for the activation of peracetic acid (PAA) compared to Cu(II) and Ag(I)). pH 3 (non-buffered acidified water) was the optimum for micropollutant abatement with the Co(II)/PAA system, while pH 5 and 7 (malic acid and bicarbonate buffers, respectively), resulted in a lower efficiency, likely due to the complexation of Co(II), which was demonstrated by speciation calculations. The optimum PAA (0.4 mM) and Co(II) (0.05 mM) concentrations reflected the maximum concentrations to avoid significant scavenging of the generated radicals by excessive PAA and Co(II). The optimum PAA and Co(II) doses were higher in comparison to Wang et al. (2020) ([PAA] = 0.1 mM, [Co(II)] ≤ 0.001 mM) or Kim et al. (2020) ([PAA] = 0.4 mM, [Co(II)] ≤ 0.02 mM), which is likely necessary due to the use of a bicarbonate buffer in the present study. However, all of the studies concluded that it is possible to perform oxidation in a practically feasible pH range of 5–7 and the required reaction time is ≤ 10 min.

The kinetics of the abatement of several *para*-substituted phenols was investigated. It could be demonstrated that a similar oxidation mechanism may occur, because the determined second-order rate constants for phenolates were correlated with the Hammett constants of the

substituents. Another feature for all studied surrogate micropollutant compounds was that the reaction rate decreased sharply after reaction times of 1–2 min. This coincided with the depletion of PAA. A subsequent second dose of PAA only led to a significant further abatement of the target compounds when it was added quickly after the first dose (≤ 1 min after the initial PAA dose). This indicates that the catalyst was deactivated (i.e., the cycling of Co(II)-Co(III) was inhibited), which was confirmed by the formation of a precipitate identified as Co(III)O(OH). The precipitation of Co(III) has also a significant impact on the reaction mechanism because the major radical species contributing to the micropollutant abatement according to previous studies, $CH_3C(O)OO^{\bullet}$, forms from the reaction of Co(III) with PAA (Kim et al., 2020; Wang et al., 2020). This could explain the somewhat poor performance of the studied Co(II)/PAA system in comparison to the earlier studies (Kim et al., 2020; Wang et al., 2020). The presence of a bicarbonate buffer could have contributed to the deactivation of the catalyst as previous studies (typically conducted in non-buffered systems) have not reported similar phenomenon. Since many real waters and wastewaters contain similar or higher concentrations of HCO_3^-, this deactivation would be expected also in real water treatment scenarios with the Co(II)/PAA system.

Preliminary experiments were carried out with a Co(II)-coated geopolymer foam as a heterogeneous catalyst for PAA activation. The use of geopolymer foam for such an application is a novel potential solution to overcome the problems of the homogenous system. The obtained abatement of phenol was close to aqueous Co(II). The leaching of Co(II) for the duration of the experiments (7 h) was very low (total 0.37% of the added Co(II)). There was also evidence that no catalyst deactivation occurred since the relative phenol abatement stayed approximately constant at 40% for 7 h using a flow rate of 1 L h^{-1}. Therefore, a solid-supported Co(II)/PAA system might be a novel option for practical water treatment under realistic conditions.

Data availability

The raw data required to reproduce these findings are available for download from https://doi.org/10.23729/371d7535-1ac5-4282-b95c-c8b1006fdc1f

Declaration of Competing Interest

The authors declare that they have no known competing financial interests or personal relationships that could have appeared to influence the work reported in this paper.

Acknowledgments

This study was supported by the Academy of Finland (grants #315103 and #326291). We thank Ulrich Bergman, Yangmei Yu, Mohammad Bhuyan, Samppa Hyvärinen, Elisa Wirkkala, Jarno Karvonen, Jani Österlund, Anu Myllymäki, Hannele Härkman, Elisabeth Muck, Ursula Schönenberger, and Urs Jans for providing assistance with the experiments. Part of the work was carried out with the support of the Centre for Material Analysis, University of Oulu, Finland. Part of the illustration was created with BioRender.com.

Supplementary materials

Supplementary material associated with this article can be found, in the online version, at doi:10.1016/j.watres.2022.118984.

References

Ao, X., Eloranta, J., Huang, C.-H., Santoro, D., Sun, W., Lu, Z., Li, C., 2021. Peracetic acid-based advanced oxidation processes for decontamination and disinfection of water: a review. Water Res. 188, 116479 https://doi.org/10.1016/j.watres.2020.116479.

Awad, M.I., Oritani, T., Ohsaka, T., 2003. Kinetic studies on the oxidation of iodide by peroxyacetic acid. Inorg. Chim. Acta 344, 253–256. https://doi.org/10.1016/S0020-1693(02)01337-3.

Bach, R.D., Ayala, P.Y., Schlegel, H.B., 1996. A reassessment of the bond dissociation energies of peroxides. An ab initio study. J. Am. Chem. Soc. 118, 12758–12765. https://doi.org/10.1021/ja961838i.

Bader, H., Sturzenegger, V., Hoigné, J., 1988. Photometric method for the determination of low concentrations of hydrogen peroxide by the peroxidase catalyzed oxidation of N,N-diethyl-p-phenylenediamine (DPD). Water Res. 22, 1109–1115. https://doi.org/10.1016/0043-1354(88)90005-X.

Bettenhausen, C.A., 2020. How peracetic acid is changing wastewater treatment. Chem. Eng. News 98.

Bianchini, R., Calucci, L., Lubello, C., Pinzino, C., 2002. Intermediate free radicals in the oxidation of wastewaters. Res. Chem. Intermed. 28, 247–256. https://doi.org/10.1163/156856702320267154.

Briancesco, R., Veschetti, E., Ottaviani, M., Bonadonna, L., 2005. Peracetic acid and sodium hypochlorite effectiveness in reducing resistant stages of microorganisms. Cent. Eur. J. Public Health 13, 159–162.

Buschini, A., Carboni, P., Furlini, M., Poli, P., Rossi, C., 2004. Sodium hypochlorite-, chlorine dioxide- and peracetic acid-induced genotoxicity detected by the Comet assay and Saccharomyces cerevisiae D7 tests. Mutagenesis 19, 157–162. https://doi.org/10.1093/mutage/geh012.

Caretti, C., Lubello, C., 2003. Wastewater disinfection with PAA and UV combined treatment: a pilot plant study. Water Res. 37, 2365–2371. https://doi.org/10.1016/S0043-1354(03)00025-3.

Chen, J., Xu, J., Liu, T., Wang, Q., Li, N., Zhang, Y., Yang, L., Zhou, X., 2022. Oxidation of tetracycline antibiotics by peracetic acid: reaction kinetics, mechanism, and antibacterial activity change. Chem. Eng. J. 431, 134190 https://doi.org/10.1016/j.cej.2021.134190.

Coyle, E.E., Ormsbee, L.E., Brion, G.M., 2014. Peracetic acid as an alternative disinfection technology for wet weather flows. Water Environ. Res. 86, 687–697. https://doi.org/10.2175/106143014X13975035525663.

De Velásquez, Ma.T.O., Yáñez-Noguez, I., Jiménez-Cisneros, B., Pabello, V.M.L., 2008. Adding silver and copper to hydrogen peroxide and peracetic acid in the disinfection of an advanced primary treatment effluent. Environ. Technol. 29, 1209–1217. https://doi.org/10.1080/09593330802270632.

Domínguez-Henao, L., Turolla, A., Monticelli, D., Antonelli, M., 2018. Assessment of a colorimetric method for the measurement of low concentrations of peracetic acid and hydrogen peroxide in water. Talanta 183, 209–215. https://doi.org/10.1016/j.talanta.2018.02.078.

Dong, J., Xu, W., Liu, S., Gong, Y., Yang, T., Du, L., Chen, Q., Tan, X., Liu, Y., 2022. Lignin-derived biochar to support $CoFe_2O_4$: effective activation of peracetic acid for sulfamethoxazole degradation. Chem. Eng. J. 430, 132868 https://doi.org/10.1016/j.cej.2021.132868.

Dong, S., Liu, Y., Feng, L., Zhang, L., 2021. Oxidation of pyrazolone pharmaceuticals by peracetic acid: kinetics, mechanism and genetic toxicity variations. Chemosphere 132947. https://doi.org/10.1016/j.chemosphere.2021.132947.

Eberhardt, M.K., Santos, C., Ann Soto, M., 1993. Formation of hydroxyl radicals and Co^{3+} in the reaction of Co^{2+}-EDTA with hydrogen peroxide. catalytic effect of Fe^{3+}. Biochim. Biophys. Acta 1157, 102–106. https://doi.org/10.1016/0304-4165(93)90084-L.

Flores, M.J., Lescano, M.R., Brandi, R.J., Cassano, A.E., Labas, M.D., 2014. A novel approach to explain the inactivation mechanism of Escherichia coli employing a commercially available peracetic acid. Water Sci. Technol. 69, 358–363.

Gao, Z., Zhang, D., Jun, Y.-S., 2021. Does tert-butyl alcohol really terminate the oxidative activity of •OH in inorganic redox chemistry? Environ. Sci. Technol. 55, 10442–10450. https://doi.org/10.1021/acs.est.1c01578.

Guo, Y., Zhan, J., Yu, G., Wang, Y., 2021. Evaluation of the concentration and contribution of superoxide radical for micropollutant abatement during ozonation. Water Res. 194, 116927 https://doi.org/10.1016/j.watres.2021.116927.

Hansch, Corwin., Leo, A., Taft, R.W., 1991. A survey of Hammett substituent constants and resonance and field parameters. Chem. Rev. 91, 165–195. https://doi.org/10.1021/cr00002a004.

Haynes, W.M. (Ed.), 2017. CRC Handbook of chemistry and physics, 97th edition. CRC Press, Taylor & Francis Group, Boca Raton, FL.

Henao, L.D., Turolla, A., Antonelli, M., 2018. Disinfection by-products formation and ecotoxicological effects of effluents treated with peracetic acid: a review. doi:10.1016/j.chemosphere.2018.09.005.

Hey, G., Ledin, A., Jansen, J.L.C., Andersen, H.R., 2012. Removal of pharmaceuticals in biologically treated wastewater by chlorine dioxide or peracetic acid. Environ. Technol. 33, 1041–1047. https://doi.org/10.1080/09593330.2011.606282.

Hoigné, J., Bader, H., 1994. Kinetics of reactions of chlorine dioxide (OClO) in water—I. Rate constants for inorganic and organic compounds. Water Res. 28, 45–55. https://doi.org/10.1016/0043-1354(94)90118-X.

Hoigné, J., Bader, H., 1983. Rate constants of reactions of ozone with organic and inorganic compounds in water—II: dissociating organic compounds. Water Res. 17, 185–194. https://doi.org/10.1016/0043-1354(83)90099-4.

Jans, U., Prasse, C., von Gunten, U., 2021. Enhanced treatment of municipal wastewater effluents by Fe-TAML/H2O2: efficiency of micropollutant abatement. Environ. Sci. Technol. 55, 3313–3321. https://doi.org/10.1021/acs.est.0c07662.

Kamath, D., Mezyk, S.P., Minakata, D., 2018. Elucidating the elementary reaction pathways and kinetics of hydroxyl radical-induced acetone degradation in aqueous phase advanced oxidation processes. Environ. Sci. Technol. 52, 7763–7774. https://doi.org/10.1021/acs.est.8b00582.

Kim, J., Du, P., Liu, W., Luo, C., Zhao, H., Huang, C.-H., 2020. Cobalt/Peracetic acid: advanced oxidation of aromatic organic compounds by acetylperoxyl radicals. Environ. Sci. Technol. 54, 5268–5278. https://doi.org/10.1021/acs.est.0c00356.

Kim, J., Huang, C.-H., 2021. Reactivity of peracetic acid with organic compounds: a critical review. ACS EST Water 1, 15–33. https://doi.org/10.1021/acsestwater.0c00029.

Kim, J., Zhang, T., Liu, W., Du, P., Dobson, J.T., Huang, C.-H., 2019. Advanced oxidation process with peracetic acid and Fe(II) for contaminant degradation. Environ. Sci. Technol. 53, 13312–13322. https://doi.org/10.1021/acs.est.9b02991.

Lalueza, P., Carmona, D., Monzón, M., Arruebo, M., Santamaría, J., 2012. Strong bactericidal synergy between peracetic acid and silver-exchanged zeolites. Microporous Mesoporous Mater. 156, 171–175. https://doi.org/10.1016/j.micromeso.2012.02.035.

Lazarova, V., Janex, M.L., Fiksdal, L., Oberg, C., Barcina, I., Pommepuy, M., 1998. Advanced wastewater disinfection technologies: short and long term efficiency. Water Sci. Technol. 38, 109–117. https://doi.org/10.1016/S0273-1223(98)00810-5.

Lee, Y., von Gunten, U., 2012. Quantitative structure–activity relationships (QSARs) for the transformation of organic micropollutants during oxidative water treatment. Water Res. 46, 6177–6195. https://doi.org/10.1016/j.watres.2012.06.006.

Lee, Y., von Gunten, U., 2010. Oxidative transformation of micropollutants during municipal wastewater treatment: comparison of kinetic aspects of selective (chlorine, chlorine dioxide, ferrateVI, and ozone) and non-selective oxidants (hydroxyl radical). Water Res. 44, 555–566. https://doi.org/10.1016/j.watres.2009.11.045.

Lin, J., Hu, Y., Xiao, J., Huang, Y., Wang, M., Yang, H., Zou, J., Yuan, B., Ma, J., 2021. Enhanced diclofenac elimination in Fe(II)/peracetic acid process by promoting Fe (III)/Fe(II) cycle with ABTS as electron shuttle. Chem. Eng. J. 420, 129692 https://doi.org/10.1016/j.cej.2021.129692.

Liu, B., Guo, W., Jia, W., Wang, H., Zheng, S., Si, Q., Zhao, Q., Luo, H., Jiang, J., Ren, N., 2021. Insights into the oxidation of organic contaminants by Co(II) activated peracetic acid: the overlooked role of high-valent cobalt-oxo species. Water Res. 201, 117313 https://doi.org/10.1016/j.watres.2021.117313.

Lubello, C., Caretti, C., Gori, R., 2002. Comparison between PAA/UV and H_2O_2/UV disinfection for wastewater reuse. Water Sci. Technol. 2, 205–212. https://doi.org/10.2166/ws.2002.0025.

Luna-Pabello, V.M., Ríos, M.M., Jiménez, B., Orta De Velasquez, M.T., 2009. Effectiveness of the use of Ag, Cu and PAA to disinfect municipal wastewater. Environ. Technol. 30, 129–139. https://doi.org/10.1080/09593330802422506.

Luukkonen, T., Heyninck, T., Rämö, J., Lassi, U., 2015. Comparison of organic peracids in wastewater treatment: disinfection, oxidation and corrosion. Water Res. 85, 275–285. https://doi.org/10.1016/j.watres.2015.08.037.

Luukkonen, T., Pehkonen, S.O., 2017. Peracids in water treatment: A critical review. Crit. Rev. Environ. Sci. Technol. 47, 1–39. https://doi.org/10.1080/10643389.2016.1272343.

Luukkonen, T., Yliniemi, J., Sreenivasan, H., Ohenoja, K., Finnilä, M., Franchin, G., Colombo, P., 2020. Ag- or Cu-modified geopolymer filters for water treatment manufactured by 3D printing, direct foaming, or granulation. Sci. Rep. 10, 7233. https://doi.org/10.1038/s41598-020-64228-5.

Marchaj, A., Kelley, D.G., Bakac, A., Espenson, J.H., 1991. Kinetics of the reactions between alkyl radicals and molecular oxygen in aqueous solution. J. Phys. Chem. 95, 4440–4441. https://doi.org/10.1021/j100164a051.

Neta, P., Huie, R.E., Ross, A.B., 1990. Rate constants for reactions of peroxyl radicals in fluid solutions. J. Phys. Chem. Ref. Data 19, 413–513. https://doi.org/10.1063/1.555854.

Niu, X., Elakneswaran, Y., Islam, C.R., Provis, J.L., Sato, T., 2022. Adsorption behaviour of simulant radionuclide cations and anions in metakaolin-based geopolymer. J. Hazard. Mater. 429, 128373 https://doi.org/10.1016/j.jhazmat.2022.128373.

Novais, R.M., Pullar, R.C., Labrincha, J.A., 2020. Geopolymer foams: an overview of recent advancements. Prog. Mater. Sci. 109, 100621 https://doi.org/10.1016/j.pmatsci.2019.100621.

Pecci, L., Montefoschi, G., Cavallini, D., 1997. Some new details of the copper-hydrogen peroxide interaction. Biochem. Biophys. Res. Commun. 235, 264–267. https://doi.org/10.1006/bbrc.1997.6756.

Schweitzer, G.K., Pesterfield, L.L., 2010. The aqueous chemistry of the elements. Oxford University Press.

SFS-EN ISO 17294-2, 2016. Water quality. Application of inductively coupled plasma mass spectrometry (ICP-MS). Part 2: Determination of 62 elements (ISO 17294-2: 2003). Finnish Standards Association SFS, Helsinki.

Shah, A.D., Liu, Z.-Q., Salhi, E., Höfer, T., von Gunten, U., 2015. Peracetic acid oxidation of saline waters in the absence and presence of H_2O_2: secondary oxidant and disinfection byproduct formation. Environ. Sci. Technol. 49, 1698–1705. https://doi.org/10.1021/es503920n.

Stefan, M.I., 2018. Advanced Oxidation Processes for Water Treatment: Fundamentals and Applications. IWA Publishing, London.

Stumm, W., Morgan, J.J., 1996. Aquatic Chemistry, Chemical Equilibria and Rates in Natural Waters, 3rd ed. John Wiley & Sons, New York.

Veschetti, E., Cutilli, D., Bonadonna, L., Briancesco, R., Martini, C., Cecchini, G., Anastasi, P., Ottaviani, M., 2003. Pilot-plant comparative study of peracetic acid and sodium hypochlorite wastewater disinfection. Water Res. 37, 78–94. https://doi.org/10.1016/s0043-1354(02)00248-8.

von Gunten, U., 2018. Oxidation processes in water treatment: are we on track? Environ. Sci. Technol. 52, 5062–5075. https://doi.org/10.1021/acs.est.8b00586.

von Sonntag, C., von Gunten, U., 2012. Chemistry of Ozone in Water and Wastewater Treatment: From Basic Principles to Applications. IWA Publishing. https://doi.org/10.2166/9781780400839.

Wang, D., Yamaki, S., Kawai, Y., Yamazaki, K., 2020. Sanitizing efficacy and antimicrobial mechanism of peracetic acid against histamine-producing bacterium, Morganella psychrotolerans. LWT 126, 109263. https://doi.org/10.1016/j.lwt.2020.109263.

Wang, J., Xiong, B., Miao, L., Wang, S., Xie, P., Wang, Z., Ma, J., 2021. Applying a novel advanced oxidation process of activated peracetic acid by $CoFe_2O_4$ to efficiently degrade sulfamethoxazole. Appl. Catal. B 280, 119422. https://doi.org/10.1016/j.apcatb.2020.119422.

Wang, S., Wang, H., Liu, Y., Fu, Y., 2020. Effective degradation of sulfamethoxazole with Fe^{2+}-zeolite/peracetic acid. Sep. Purif. Technol. 233, 115973 https://doi.org/10.1016/j.seppur.2019.115973.

Wang, Z., Fu, Y., Peng, Y., Wang, S., Liu, Y., 2021. HCO_3^-/CO_3^{2-} enhanced degradation of diclofenac by Cu(II)-activated peracetic acid: efficiency and mechanism. Sep. Purif. Technol. 277, 119434 https://doi.org/10.1016/j.seppur.2021.119434.

Wang, Z., Wang, J., Xiong, B., Bai, F., Wang, S., Wan, Y., Zhang, L., Xie, P., Wiesner, M. R., 2020. Application of cobalt/peracetic acid to degrade sulfamethoxazole at neutral condition: efficiency and mechanisms. Environ. Sci. Technol. 54, 464–475. https://doi.org/10.1021/acs.est.9b04528.

Wu, W., Tian, D., Liu, T., Chen, J., Huang, T., Zhou, X., Zhang, Y., 2020. Degradation of organic compounds by peracetic acid activated with Co_3O_4: a novel advanced oxidation process and organic radical contribution. Chem. Eng. J. 394, 124938 https://doi.org/10.1016/j.cej.2020.124938.

Zhang, C., Brown, P.J.B., Hu, Z., 2019. Higher functionality of bacterial plasmid DNA in water after peracetic acid disinfection compared with chlorination. Sci. Total Environ. 685, 419–427. https://doi.org/10.1016/j.scitotenv.2019.05.074.

Zhang, T., Huang, C.-H., 2020. Modeling the kinetics of UV/peracetic acid advanced oxidation process. Environ. Sci. Technol. 54, 7579–7590. https://doi.org/10.1021/acs.est.9b06826.

Zhang, Y.J., Han, Z.C., He, P.Y., Chen, H., 2020. Geopolymer-based catalysts for cost-effective environmental governance: a review based on source control and end-of-pipe treatment. J. Clean. Prod. 263, 121556 https://doi.org/10.1016/j.jclepro.2020.121556.

Zhou, X.-F., 2017. Degradation and mineralisation of 2,4-dichlorophenol by ultrasonic-assisted AOPS using oxidants coupled with silver sulphate. Oxid. Commun. 40, 1025–1034.